Journal Pre-proof

A versatile lead iodide particle synthesis and film surface analysis for optoelectronics

Nasir Awol, Chernet Amente, Gaurav Verma, Jung Yong Kim

PII: S0925-8388(20)30849-5

DOI: https://doi.org/10.1016/j.jallcom.2020.154486

Reference: JALCOM 154486

To appear in: *Journal of Alloys and Compounds*

Received Date: 29 January 2020

Revised Date: 16 February 2020

Accepted Date: 22 February 2020

Please cite this article as: N. Awol, C. Amente, G. Verma, J.Y. Kim, A versatile lead iodide particle synthesis and film surface analysis for optoelectronics, *Journal of Alloys and Compounds* (2020), doi: https://doi.org/10.1016/j.jallcom.2020.154486.

The experiments were designed by N.A., G.V. and J.Y.K. and executed by N.A. All the authors helped in conceptualizing the work. Data was analyzed and interpreted by N.A., G.V. and J.Y.K. The manuscript was conceived, written and finalized by N.A., G.V. and J.Y.K.

A Versatile Lead Iodide Particle Synthesis and Film Surface Analysis for Optoelectronics

Nasir Awol,[a,b] Chernet Amente,[c] Gaurav Verma,[b,d,*] Jung Yong Kim[a,e,*]

a. *School of Materials Science and Engineering, Jimma University Institute of Technology, Jimma University. P.O. Box 378, Jimma, Ethiopia*
b. *Dr. Shanti Swarup Bhatnagar University Institute of Chemical Engineering and Technology, Panjab University, Chandigarh, 160014,India*
c. *Department of Physics, College of Computational and Natural Science, Addis Ababa University, P.O. Box 1176, Addis Ababa, Ethiopia*
d. *Centre for Nanoscience & Nanotechnology, University Institute for Emerging Areas in Science and Technology, Panjab University, Chandigarh, 160014, India*
e. *School of Chemical Engineering, Jimma Institute of Technology, Jimma University, P.O. Box 378, Jimma, Ethiopia*

* Corresponding authors:

E-mail: gauravverma@pu.ac.in;Tel: +91-9872492858 (G.V.)

E-mail: jungyong.kim@ju.edu.et;Tel: +251-931461907(J.Y.K.)

ORCID

0000-0002-1894-1103 (G.V.)

0000-0002-7736-6858 (J.Y.K.)

Abstract

Lead (II) iodide, PbI_2, semiconductor was synthesized using versatile methods such as hydrothermal, refluxing, solid-state reaction, and co-precipitation for optoelectronics. All the PbI_2 particles exhibited hexagonal-layered 2H structure in which the average crystallite size and optical bandgap (E_g) were57±10 nm and 2.31 eV, respectively. Then, PbI_2films were prepared using dimethyl sulfoxide (DMSO) or dimethylformamide (DMF) on the top of a mesoporous TiO_2 layer, yielding a wider E_g of 2.33-2.36. Finally, through water contact angle measurement, the surface and interfacial properties of the thin film were characterized, exhibiting initial solid-vapor surface tension (γ_{sv}) of 6.1-6.4 mJ/m^2 and solubility parameter (δ) of 4.51-4.62$(cal/cm^3)^{1/2}$. However, when these PbI_2 films were exposed to H_2O molecules in air, δ changes from 4.62 to 7.28 $(cal/cm^3)^{1/2}$ for PbI_2 (DMSO) film or 4.51 to 12.98$(cal/cm^3)^{1/2}$ for the PbI_2 (DMF) film, respectively. Finally, by employing the theory of melting point depression combined with the Flory-Huggins lattice theory, the interfacial interactions between PbI_2 and regioregular poly (3-hexylthiophene-2,5-diyl) were qualitatively characterized. The smaller the χ interaction parameter, the more depressed the melting point.

Key words: Lead iodide; Surface; Interface; Optoelectronics; Flory-Huggins Theory; Melting Point Depression.

1. INTRODUCTION

Lead (II) iodide, PbI_2, is a direct wide bandgap (E_g> 2 eV) semiconductor with a large atomic number (Z_{Pb} = 82 and Z_I = 53), displaying a heavy molecular weight of 460.81 g/mol and density of 6.2 g/cm^3[1-5].In the solid state, it shows a quasi two-dimensional structure stacked by weak van-der Waals interactions [6-11]. Hence, it exhibits polymorphisms such as 2H, 6H, and 12R, in which H and R represent hexagonal and rhombohedral, respectively [12]. Herein, various structures, called polytypes, are ascribed to the change of each layer's relative orientational order in the **c**-crystallographic direction [13,14]. Also, its layered structure allows the accommodation of small foreign molecules into the interstitial space in I-Pb-I layers [15-17].

From the 1970s, PbI_2 has been used as a nuclear particle detector such as x- and γ-ray, because it shows high absorption and carrier collection with minimized noise, depending on its bandgap, charge mobility (μ), and lifetime (τ) [18-27]. However, in 2009, Miyasaka et al. applied it into the emerging photovoltaic (PV) field by using it as a perovskite precursor, in which organometal halide perovskites have a chemical formula of ABX_3, in which A^+ = $CH_3NH_3^+$; B^{2+} = Pb^{2+}; and X^- = I^- or a halide mixture, respectively [28]. Then, after a surge of research interests [29-32], the power conversion efficiency of perovskite PV devices reached 25.2%, comparable to the conventional silicon or thin film solar cells [33].

In this study, we synthesized PbI_2 particles using various methods such as hydrothermal, refluxing, solid-state reaction, and co-precipitation. Then we characterized the optical and structural properties. Finally, we studied the surface properties (e.g., morphology, surface tension, solubility parameter) of nanostructural PbI_2 film deposited on the top of a mesoporous TiO_2 substrate, dependent on the processing solvents dimethyl sulfoxide (DMSO) and dimethyl amide (DMF). Specifically, we found that the solid-vapor surface

tension (γ_{sv}) of PbI_2 films changed with time when exposed to H_2O molecules in air. These changes were quantified by estimating solubility parameters from the water contact angle measurements. Then we studied the interfacial interactions between PbI_2 film and regioregular poly (3-hexylthiophene-2,5-diyl) (r-reg P3HT), based on the theory of melting point depression combined with Flory-Huggins theory [34]. Our results suggest that the surface and interface of PbI_2 films as a function of the solvent, DMSO and DMF, can be used for optoelectronic applications such as solar cells, lasers, light-emitting diodes, and radiation detectors. Specifically, our research is intended to understand the PbI_2 thin-film properties, applicable to a two-step sequential deposition technique for perovskite solar cells.

2. Experimental Section

2.1 Materials and Methods

In all synthesis methods, analytical grade high purity reagents were used. A stoichiometric ratio of 0.03 M of lead nitrate [$Pb(NO_3)_2$] and 0.06 M of potassium iodide (KI) were used as starting materials for all methods. For a modified hydrothermal method, samples were placed in two separate beakers with 50 mL double distilled water each, stirred and sonicated at a temperature of 70ºC for 2 hours. The two colorless solutions were kept together in another beaker and stirred for 30 minute at 100°C. The yellow solution was centrifuged, and the resulting precipitated powders were collected and dispersed in 15 mL of double-distilled water, then transferred into a 30 mL Teflon-lined autoclave. Triton X-100 (5%) was used as a nonionic surfactant. The autoclave was maintained at 200°C for 6 hours and the PbI_2 solution was cooled down at room temperature. Finally it was centrifuged, dried, and collected for further study.

For the refluxing method, a stoichiometric amount of $Pb(NO_3)_2$ and KI in 50 mL of deionized (DI) water each were weighed and added into a round bottom flask attached with a reflux condenser secured with a clamp. Then it was stirred and followed by heating at 100ºC for 6 hours. After centrifuging, the precipitated powder was collected and washed in DI water three times. The powder was annealed at 100°C for 30 minutes, and collected for further study.

For the co-precipitation method, the same stoichiometric amount of initial materials was used in another beaker with 50 mL of DI water each. The samples were continuously stirred and sonicated in separate beakers for 2 hours with a temperature of 70ºC. Then, the solutions were put together and stirred again for 2 more hours. The yellow solution was centrifuged and washed three times by DI water. Finally the powder was annealed at 100°C inside a hot air oven.

For solid-state reaction or mixture, a stoichiometric amount of $Pb(NO_3)_2$ and KI were weighed and were mixed in a jar and shaken for 6hours. The formed yellow powders were then placed into a flask containing double-distilled water to speed up the whole reaction followed by stirring for 30 minutes. The precipitate was centrifuged and rinsed by DI water and acetone three times and annealed at 100°C for 2 hours. The product was then collected for characterization. Finally, for comparison, commercially available PbI_2 powders from Tokyo Chemical Industry (TCI) in Japan were used and named as *commercial reference*.

2.2 Thin film preparation

To study the effect of solvents (DMSO and DMF) on the film-forming properties, we prepared 1M of PbI_2 solution (i.e., 460.81mg/mL of DMF or DMSO) and stirred at 70°C for 12 hours. Glass substrates were washed with detergent, DI water and ethanol in an ultrasonic

bath. Then, on the top of this glass substrate, compact titanium dioxide (c-TiO_2) and mesoporous TiO_2 (mp-TiO_2) were spin-coated. Subsequently, the mp-TiO_2/c-TiO_2/glass substrate was annealed at 500ºC for 2hours. After filtering with a 2µm polytetrafluoroethylene (PTFE) syringe filter, the PbI_2 solution (with solvent of DMSO or DMF) was spin coated on the top of mp-TiO_2/c-TiO_2/glass substrate and annealed at the temperature of 100ºC. Optical, electrical, structural and surface properties were analyzed accordingly. Note that, in this work, the PbI_2 films will be denoted by PbI_2(DMSO) film or PbI_2(DMF) film depending on the solvent used, i.e., DMSO or DMF, respectively.

2.3 Characterization

Ultraviolet-visible (UV-vis) spectra (Shimadzu UV-2600-Series) were taken using the powders in the form of solid-state pellets, for which $BaSO_4$ was used as a reference. The X-ray diffraction (XRD) measurements were carried out using a Philips X'pert PRO-240mm diffractometer with an integrated germanium detector, having a Cu-Kα radiation source at λ =1.54060 Å operating at an applied voltage of 45kV with a current intensity of 40 mA. The equatorial scans in continuous mode were taken from 2θ =4 to 80 degrees at a step of 0.017° with a scan step time of 24.4 seconds. Functional groups were identified by using a Spectrum 400 Fourier-Transform infrared (FT-IR) spectrophotometer (Perkin Elmer's, USA) at a resolution of 0.4cm^{-1}.The photoluminescence (PL) spectra were obtained by F-7000 fluorescence spectrophotometer (Hitachi, Japan), using a xenon lamp at the wavelength of 532 nm at a scan speed of 1200 nm/min. Morphologies were investigated by field-emission scanning electron microscopy (FE-SEM; Hitachi, Japan,SU8000 Series) at an accelerating voltage of 5.0 kV. For elemental analysis, the energy-dispersive x-ray spectroscopy (EDX) was carried out with an XFlash6/30 SDD detector (Bruker, Germany) with a magnification of 60kX, an operating voltage of 15 kV and an active area of 15 mm^2. Surface-mapping analysis

was performed to obtain elemental distribution in a PbI_2 film (DMSO or DMF). Water contact angle measurements were carried out by using a goniometer (KRUSS- GmbH, DSA25; Germany), for which the data was obtained in a time interval of 40 ms over a period of 30 seconds.

3. Results and Discussion

Figure 1a shows the photographic images of PbI_2 powder samples, among which the sample from the solid-state reaction shows dark yellow and the others light-yellow. However, when we examined UV-vis absorption spectra for the power samples in a solid-state pallet with the reference of $BaSO_4$, all of them exhibit an optical bandgap (E_g) of 2.31 eV at the wavelength of 537 nm, indicating that the PbI_2 bulk samples exhibit the same electronic structure. Figure S1 in the Supplementary Material (SM) shows the FT-IR spectra for these samples, in which various mode of vibration of hydroxyl group from absorbed H_2O molecules are observed: asymmetric and symmetric stretch of O-H at 3600-2800 cm^{-1} and symmetric bend (deformation) vibration of water at 1593 cm^{-1}, respectively [35,36]. Figure S2 shows the PL spectra for these samples, in which the emission peaks are observed at 501.4 ± 4.3 nm.

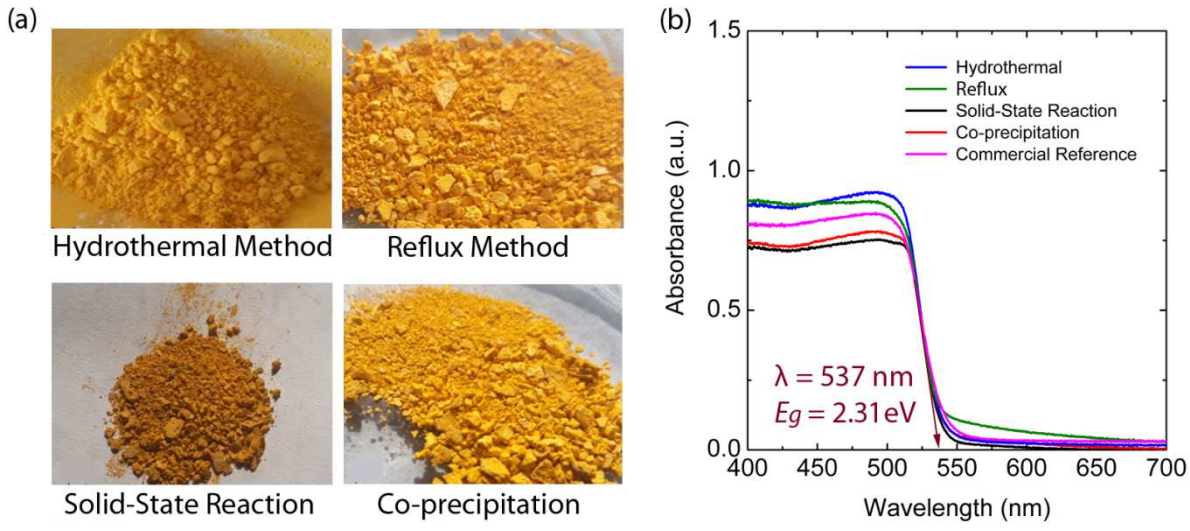

Figure 1.(a) PbI_2 powder samples from various methods such as hydrothermal, reflux, solid-state reaction and co-precipitation.(b) UV-vis absorption spectra for PbI_2 power sample in the form of solid-state pallet with the reference of $BaSO_4$.

Figure 2a shows the XRD pattern of powder samples for each processing method, all of which indicate hexagonal close packing (HCP) (Fig. 2b). Here, based on Bragg's theory ($d = \lambda/2\sin\theta$), in which d is d-spacing in nm, λ is x-ray wavelength (= 0.154 nm), and θ is scattering angle, respectively, we can estimate $\mathbf{a} = \mathbf{b} = 0.154/\left[2\sin\left(22.534/2\right)\right]\cdot 2/\sqrt{3}$ = 0.455 nm, and $\mathbf{c} = 0.154/\left[2\sin\left(12.684/2\right)\right]$ = 0.697 nm in Fig. 2b, confirming that the PbI_2 has the 2H structure among polytypism or polymorphism. Here, 2θ = 22.534° and 12.684° come from (100) and (001) crystallographic planes, respectively. Also note that in **a** and **b** calculation, the multiplication of $2/\sqrt{3}$ comes from the difference between the direction [100] and the vector **a** by the angle of 30° (see Fig. 2b, the right corner at the bottom).This estimation is well matching to the literature report with **a** = **b** = 0.4557 nm and **c** = 0.6979 nm, respectively [37].

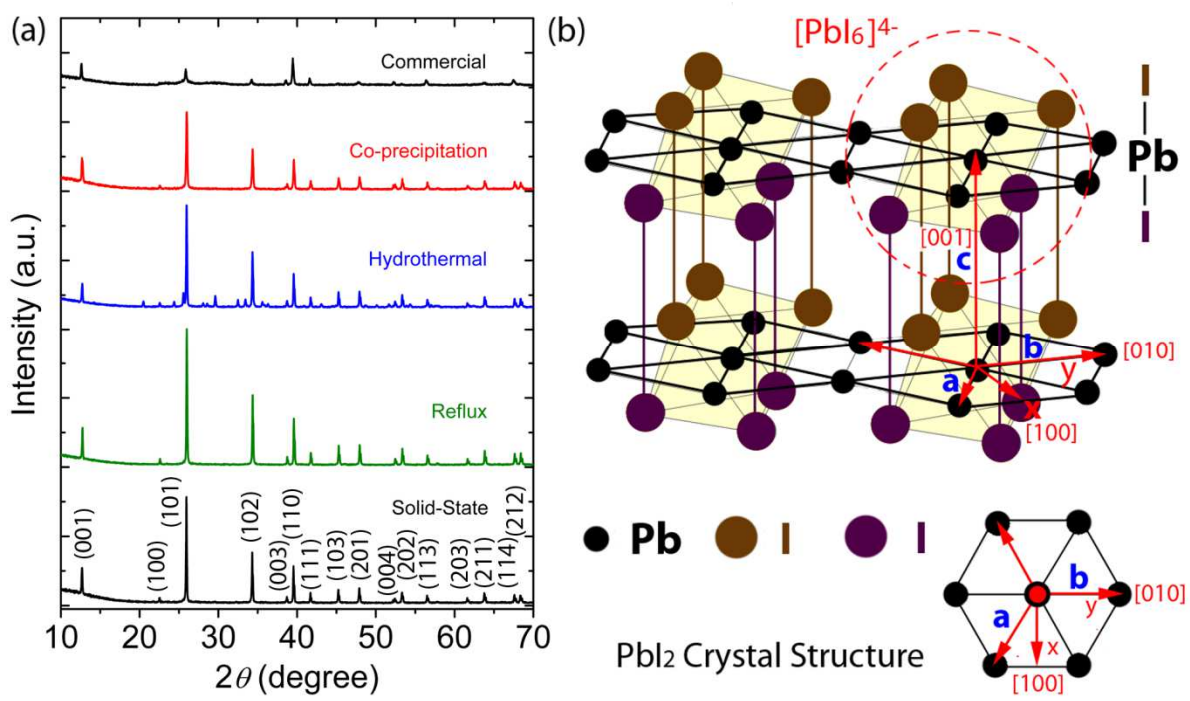

Figure 2 (a) XRD Spectra of the PbI_2 powder samples. (b) Hexagonal close packing (HCP) structure of PbI_2 crystals, in which each Pb atom forms an octahedral arrangement $[PbI_6]^{4-}$ with 6 I atoms. Polytype is 2H, in which H denotes hexagonal.

Importantly, all the samples from the four synthesis methods in this study are observed to have a better organized crystal structure than the commercial reference. The sharper XRD peaks from the constructive interference of x-ray light are clearly observed in these four methods, compared to those from the reference sample. In this condition, to clarify the crystallite size (i.e., average single-crystal domain size in PbI_2 bulk polycrystals), we employed the Scherrer's relation [38],

$$t = \frac{0.9\lambda}{\beta \cos\theta} (1)$$

where t is crystallite size, 0.9 is Scherrer's constant, β is full width at half maximum (FWHM), and θ is Bragg's diffraction angle. When we examine the (101) crystallographic plane, the crystallite size of each samples are 67 nm for solid-state reaction, 65 nm for reflux,

60 nm for hydrothermal, 47 nm for co-precipitation, and 46 nm for commercial reference. Hence, the average crystallite size of PbI_2 bulk polycrystals is 57 ± 10 nm. See Table 1 for t and β values, when λ = 1.54 nm and at θ = 13°.

Table 1. Crystallite size (t) of PbI_2 as a function of each processing method at θ = 13°, i.e., (101) crystallographic plane.

	Solid-State	Reflux	Hydrothermal	Co-precipitation	Commercial
β (radians)	0.00213	0.00220	0.00238	0.00301	0.00313
t (nm)	67	65	60	47	46

As explained in the XRD data, all the PbI_2 samples exhibit the same hexagonal 2H polytype structure with a minor difference in crystal size. Hence, we chose the PbI_2 sample from the common hydrothermal method for studying the effect of solvent on the properties of PbI_2 film. Figure 3a shows the chemical structures of two dipolar aprotic solvents DMSO [$(CH_3)_2S{=}O$] and DMF [$(CH_3)_2N\text{-}C(=O)H$]. Using these solvents, the PbI_2 solutions were prepared as shown Fig. 3b (upper image). Then PbI_2 films were deposited on the top of an mp-TiO_2/c-TiO_2/glass substrate. As shown in Fig. 3b's vial image, DMSO and DMF solutions are turbid (or partially translucent) and transparent, respectively, indicating that DMSO and DMF solutions are phase-separated and one-phase, respectively. Note that Miyamae *et al*. [2] reported that saturated PbI_2/DMSO solution may yield a colorless needle-like crystal of PbI_2. Thus, the phase separated structure might be related with the nucleation and growth (i.e., crystallization) of PbI_2 in DMSO and/or co-crystallization of the PbI_2-DMSO adduct. Using these two different solutions, we fabricated the PbI_2 films, and the macroscopic appearance is shown in Fig. 3b (lower images).The PbI_2 film (DMSO) shows a greenish yellow, whereas the film (DMF) displays transparent yellow, a memory effect from

the solution state. Herein the greenish yellow indicates that DMSO remains in this film through the co-ordination reaction between PbI_2 and DMSO (i.e., a Lewis base).

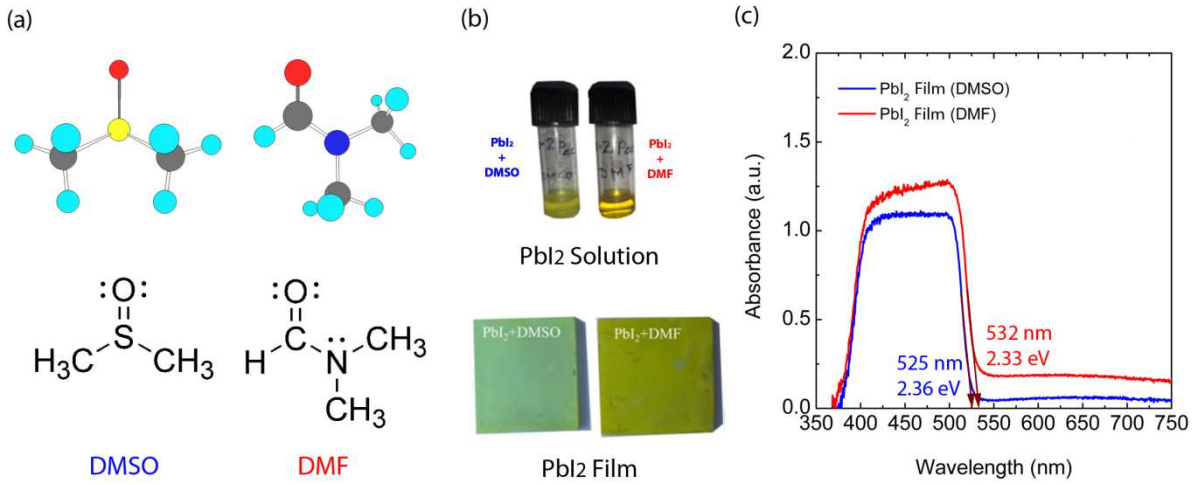

Figure 3.(a) Chemical structures of DMSO and DMF. (b) Photo images of 1MPbI_2 solutions (461.78mg/ml) and films. (c) UV-Vis absorption spectra of PbI_2 films incorporating DMSO or DMF solvent. Inset: the vials of PbI_2 solutions with DMSO (left) or DMF (right) solvent.

Figure 3c shows the UV-vis spectra for PbI_2 films, which show an optical bandgap at 2.36 eV (DMSO) and 2.33 eV (DMF), respectively. Hence, a small blue-shift is observed when compared to E_g = 2.31 eV for the PbI_2 bulk polycrystals in Fig. 1b, suggesting that the PbI_2 film on the top of an mp-TiO_2 substrate is comprised of nanoparticles. If the particle size is below the value of Bohr radius of exciton, the quantum size and confinement effect is usually observed [39]: the smaller the particle size, the wider the bandgap. As shown in the SEM images in Figure 4, the PbI_2 film (DMSO) shows clear nanostructural morphology with appreciable uniformity, whereas the film (DMF) displays serious structural deficiencies.

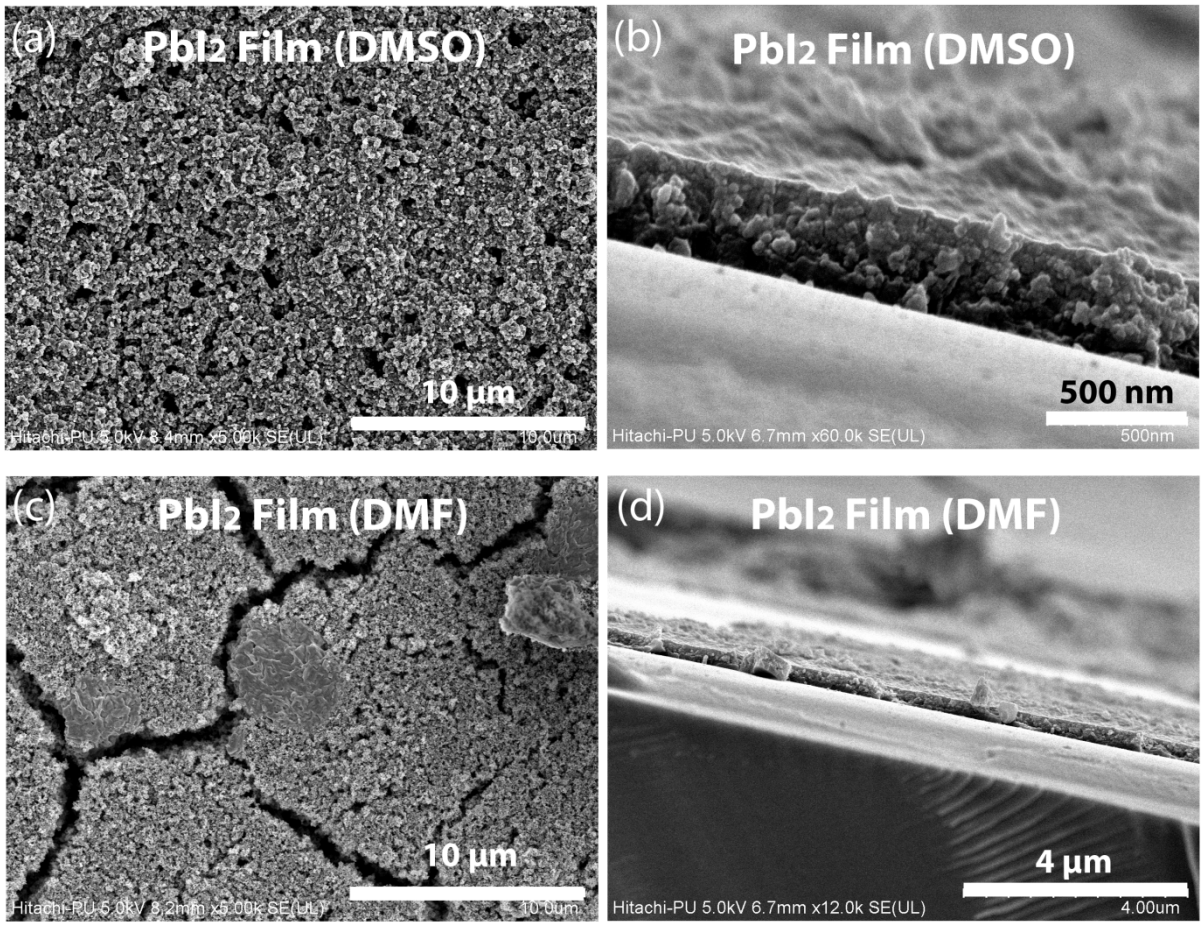

Figure 4.FE-SEM image of the PbI_2film deposited on the top of mesoporous TiO_2layer: (a) the surface image ofPbI_2film (DMSO), (b) the cross sectional view of PbI_2film (DMSO),(c) the surface image ofPbI_2film (DMF), and (d) the cross sectional view of PbI_2film (DMF).

Figure5 shows the nanoscale SEM images for the PbI_2 films. Although the PbI_2 (DMSO) film is made from a phase-separated solution containing pre-aggregate, the DMSO's characteristics such as higher polarity (P= 0.444), dielectric constant (ε= 46.829), solubility parameter [δ= 14.5 $(cal/cm^3)^{1/2}$], and boiling point (b.p.= 189 °C) [40,41], may allow for stronger interactions between Pb^{2+} ions and the O=S group in DMSO, retarding crystallization for better uniformity. On the other hand, DMF has P = 0.386, ε= 37.219, δ= 12.1 $(cal/cm^3)^{0.5}$, and b.p. = 153 °C[40,41], which is known to be toxic and allows for a wet PbI_2 film to undergo a quick evaporation of DMF molecules during the drying processes (see,

Table 2 for more information about DMSO and DMF solvents). However, it is noteworthy that, for perovskite films, DMSO and DMF are usually used together in a mixed state for dissolving organic-inorganic perovskite precursors [29].

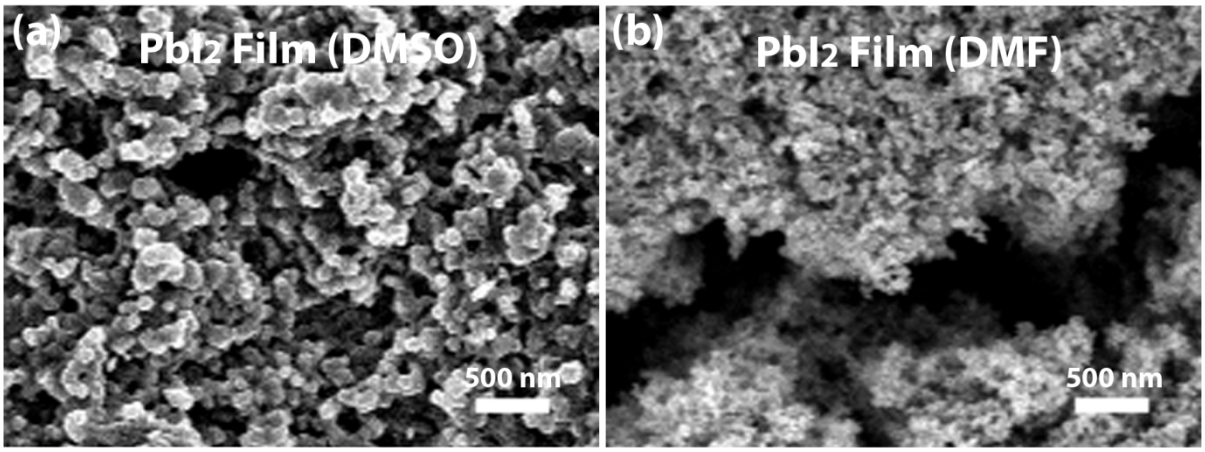

Figure 5.FE-SEM images of the PbI_2film deposited on the top of mesoporous TiO_2layer: (a) a nanostructural PbI_2 film (DMSO) and (b) a PbI_2 film (DMF) with crack morphology.

Table 2.Properties of DMSO and DMF solvents [40,41]. Here, b.p. and m.p. stand for boiling and melting points, respectively.

	b.p. (°C)	Density (g/cm^3)	Molar mass	Formula	m.p. (°C)	δ* $(cal/cm^3)^{1/2}$	δ $(MPa^{1/2})$	Relative Polarity	ε
DMSO	189	1.1	78.13	C_2H_6OS	19	14.5	29.70	0.444	46.826
DMF	153	0.944	73.09	C_3H_7NO	-61	12.1	24.78	0.386	37.219

*Note that $(cal/cm^3)^{1/2}$is normally used for the dimension of δ in thermodynamics.

Figure 6 shows the element-mapping images for the PbI_2 films processed using DMSO or DMF. Here, Pb, I, and Ti elements are yellow, white and red, respectively. As shown in this figure, in the case of PbI_2 (DMF), not only cracks, but also Pb aggregates are clearly observed, indicating non-uniform nucleation and growth of PbI_2crystals in DMF medium. For

clarity, Figure 7 show sthe additional single element mapping for Pb, I and Ti, respectively. Further information about the elemental analysis for PbI_2 films is included in Figure S3,and Tables S1 and 2 in SM.

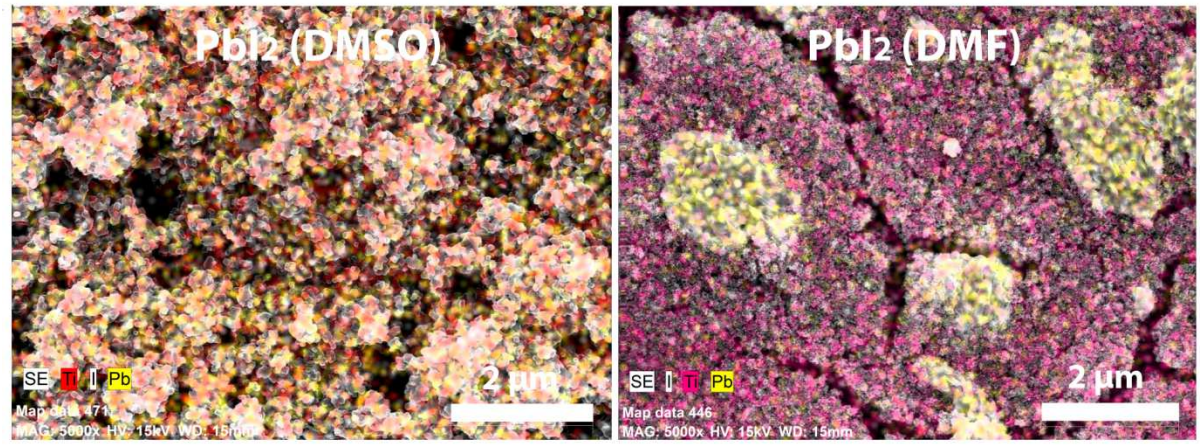

Figure 6. Mapping images of PbI_2films on the top of mp-TiO_2 layer.(a) PbI_2 (DMSO) film.(b) PbI_2 (DMF) film. Herein, Pb, I, and Ti are mapped together. Pb is yellow, I is white and Ti is red, respectively. Scale bar is 2 μm.

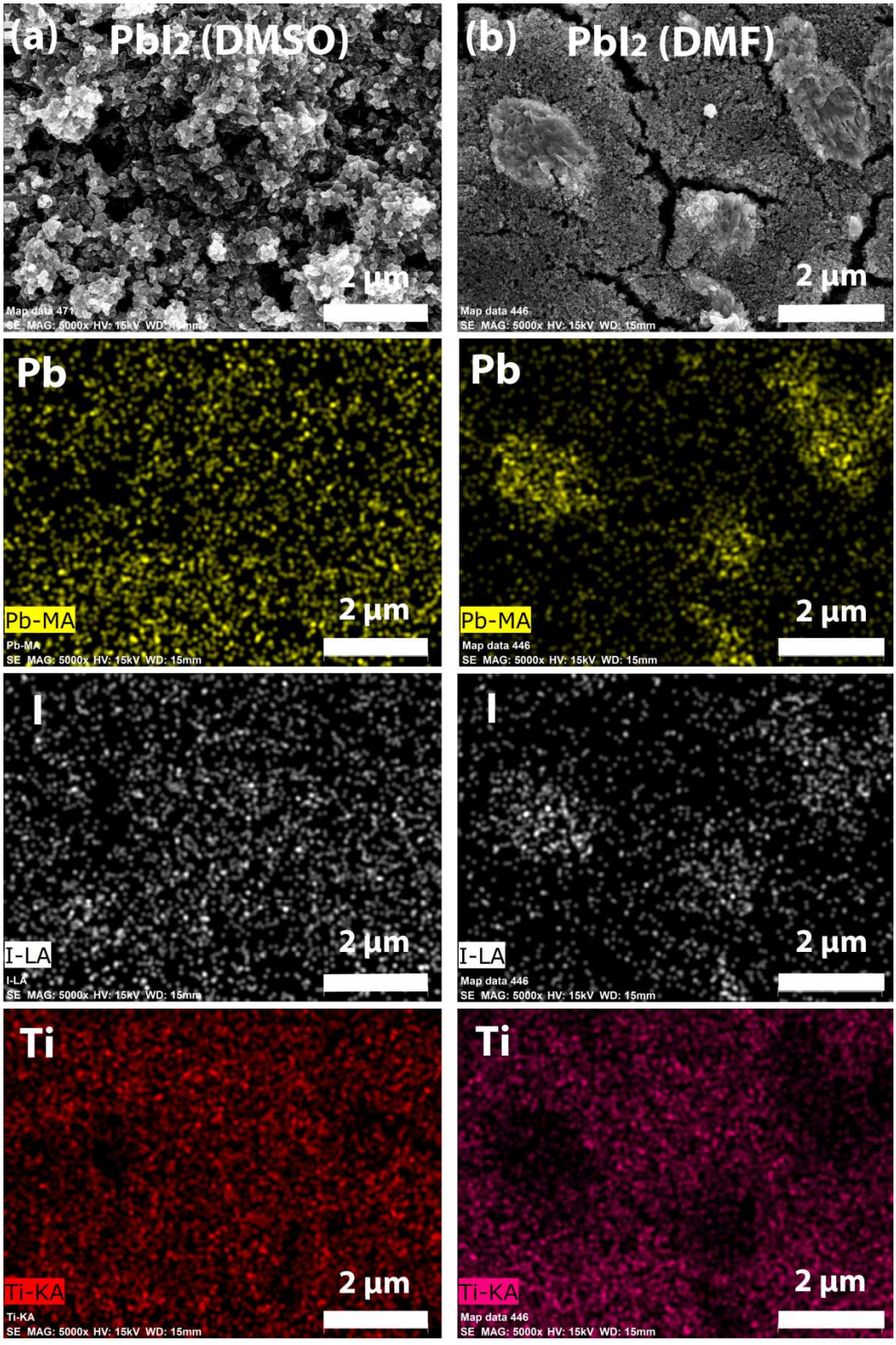

Figure 7.Elemental-mapping images of PbI_2 films on the top of an mp-TiO_2 layer. Column (a): PbI_2 (DMSO). Column (b): PbI_2 (DMF) films. Herein, Pb is yellow, I is white, and Ti is red, respectively. Scale bar is 2 µm.

Figure 8 shows the water contact angle measurement for PbI_2 films depending on the solvents, DMSO and DMF. As shown in Fig. 8a, at the first step, both films show similar contact angles, 130.08° for PbI_2 (DMSO) and 130.82° for PbI_2 (DMF), respectively. However, with increasing steps, approaching the 18th step (i.e., a saturation level), the contact angle becomes 110.95° for PbI_2 (DMSO) and 55.21° for PbI_2 (DMF), respectively. Here, the drastic change in contact angle in the PbI_2 film (DMF) may mainly originate from the crack morphology as shown in Figs. 4c and 5b. Importantly, the surface of PbI_2 in contact with H_2O and O_2 could undergo the reactions of $PbI_2+O_2 = PbO + I_2$; $PbI_2 + 2H_2O = 2HI + Pb(OH)_2$; and $PbI_2 + H_2O = [PbI_2(H_2O)]$, etc. Also note that not only the solvents (DMSO and DMF) are hygroscopic, but also PbI_2 is known to have solubility in water, 0.0756 mg/mL at 20 °C, and 0.4100 mg/mL at 100 °C, respectively [1,42].

For utilizing PbI_2as an underlying layer in the sequential deposition method for perovskite solar cells [32] and other optoelectronics, we need to know the surface property in terms of surface tension and the solubility parameter, providing wettability, adhesion, orthogonality of solvent, and other interfacial interactions. For this purpose, we may rely on Li and Newmann's relation [43,44]:

$$\cos\theta = -1 + 2\sqrt{\frac{\gamma_{sv}}{\gamma_{lv}}}e^{-\beta(\gamma_{lv}-\gamma_{sv})^2} \qquad (2)$$

where θ is contact angle, and β is the constant = 0.000115 $(m^2/mJ)^2$. γ_{sv} and γ_{lv} are the surface tension of solid-vapor and liquid-vapor, respectively. Then, we may roughly estimate δ through the known relation, $\delta\left[\left(cal/cm^3\right)^{1/2}\right] = 1.829058\sqrt{\gamma_{sv}}$ [45-47]. The results are summarized in Table 3. Hence, the surface of PbI_2 film is initially very hydrophobic with $\delta \approx 4.5 - 4.6\,(cal/cm^3)^{1/2}$. However, by contacting with water in air, the surface is changed to become more hydrophilic [$\delta \approx 13.0\,(cal/cm^3)^{1/2}$] in the case of PbI_2 (DMF), whereas the PbI_2 film from DMSO solvent still remains hydrophobic with $\delta \approx 7.3\,(cal/cm^3)^{1/2}$. Table 3 shows

the all the results of δ estimation. Note that, for a comparison purpose, r-reg P3HT and regiorandom P3HT (r-ran P3HT) have the solubility parameter of 8.72 and 10.50$(cal/cm^3)^{1/2}$, respectively [46,47].

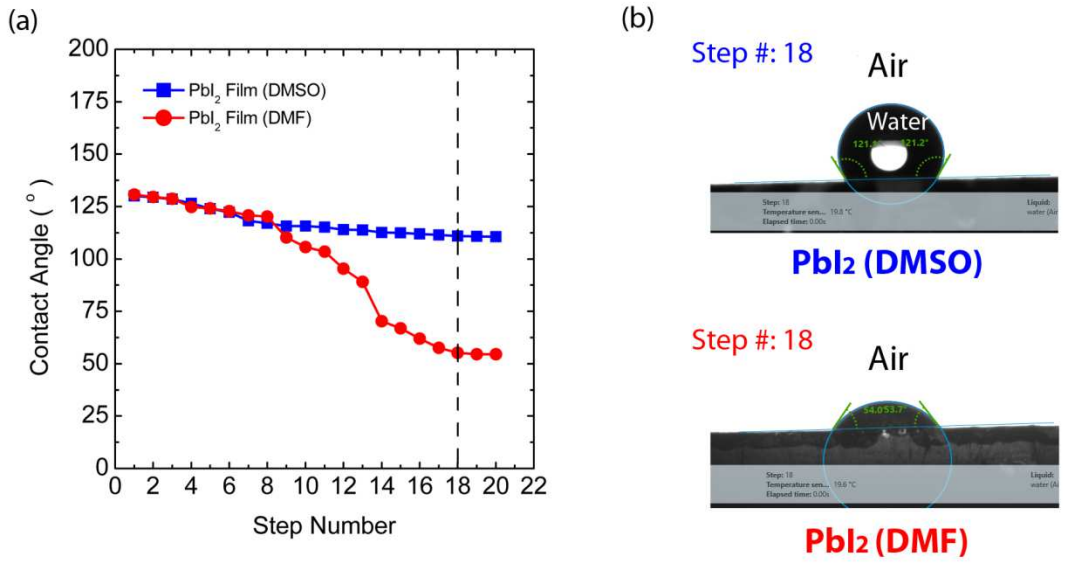

Figure 8.(a) Water contact angle as a function of step number. (b) Contact angle of PbI_2 films made from DMSO and DMF, respectively, at step number 18.

Table 3.Contact angle (θ), solid-vapor surface tension (γ_{sv}), and solubility parameter (δ) for PbI_2 films, when DMSO or DMF is used as a solvent.

Step Number	PbI_2 Film (DMSO)				PbI_2 Film (DMF)			
	θ (°)	γ_{sv} mJ/m^2	δ $(cal/cm^3)^{1/2}$	δ $MPa^{1/2}$	θ (°)	γ_{sv} mJ/m^2	δ $(cal/cm^3)^{1/2}$	δ $MPa^{1/2}$
1	130.07499	6.37176	4.61708	9.45855	130.81797	6.07804	4.50941	9.23798
18	110.95393	15.83957	7.27963	14.91305	55.20461	50.39263	12.98437	26.59978

For understanding the physical meaning of the surface properties of PbI_2 film (DMSO or DMF), we investigated the interfacial interactions between r-reg P3HT and PbI_2 by putting the polymer on the top of PbI_2 film (Figure 9).

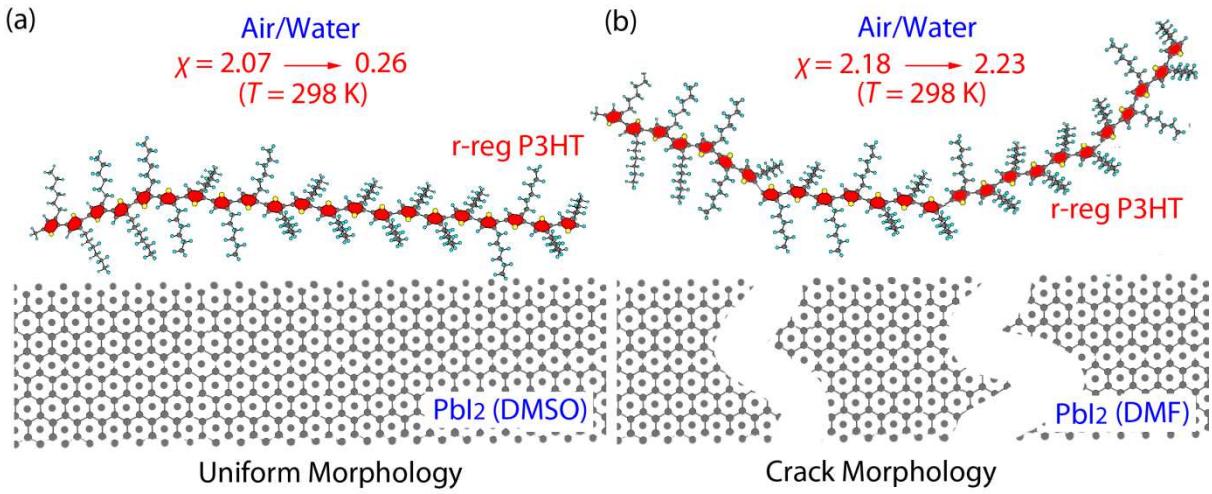

Figure 9.Schematic drawing of r-reg P3HT on the PbI_2 film with hexagonal close packing structure. (a) PbI_2 (DMSO) film with a uniform morphology (e.g., hydrophobic surface). (b) PbI_2 (DMF) film with a crack-morphology (e.g., hydrophilic surface).

To this end, the first calculation is the Flory-Huggins interaction parameter (χ) [48],

$$\chi = \frac{\hat{V}_1}{RT}\left(\delta_1 - \delta_2\right)^2 \qquad (3)$$

where $\hat{V}_1 = M_1/\rho_1 = \left(461.01\,\mathrm{g/mol}\right)/\left(6.61\,\mathrm{g/cm^3}\right) = 74.84\,\mathrm{cm^3/mol}$ is the molar volume of PbI_2, R = 1.987 cal/(K·mol) is the gas constant, and T (K) is the absolute temperature. δ_1 and δ_2 are solubility parameters of PbI_2 and r-reg P3HT, respectively. Note that the components, 1 and 2 are PbI_2 and r-reg P3HT, respectively. Based on the contact angle data, the results are summarized in Table 4. Specifically, when T is 298 K, the χ value for the r-reg P3HT:PbI_2 system (DMSO) is 2.07 (for step no. 1) and 0.26 (for step no. 18), respectively, indicating that the PbI_2 film (DMSO) will show excellent wettability with r-reg P3HT, when PbI_2 is exposed to water and air. Note that when χ is less than 0.5, it is usually a miscible system in polymer science [34,48]. On the other hand, at that same temperature of 298 K, the

χ value for r-reg P3HT:PbI_2 system (DMF) is 2.19 (for step no. 1) and 2.23 (for step no. 18), respectively, indicating that, although PbI_2 film's surface changed drastically from hydrophobic to hydrophilic, the relative difference between two solubility parameters are comparable, leading to the similar χ value of ca. 2.2 (i.e., dewetting is expected).

Table 4.Flory-Huggins χ interaction parameter for binary r-reg P3HT/PbI_2 system, when PbI_2 films were processed using DMSO or DMF solvent, respectively.

	r-reg P3HT/PbI_2 System (DMSO)		r-reg P3HT/PbI_2 System (DMF)	
Step Number	1	18	1	18
χ	616.34 K/T	76.03 K/T	649.85 K/T	665.38 K/T

Furthermore, based on the theory of melting point depression combined with the Flory-Huggins theory, we may examine qualitatively the effect of χ on the melting behavior of r-reg P3HT:PbI_2 system [34, 46, 47].

$$\frac{1}{T_m}-\frac{1}{T_m^0}=\frac{R}{\Delta H_u}\frac{V_u}{\hat{V}_1}\left(\phi_1-\chi\phi_1^2\right) \qquad (4)$$

where T_m and T_m^0 (= 490.2 K) are the melting temperature of r-reg P3HT with the PbI_2 and the melting temperature of pure P3HT. ΔH_u (= 47.5 J/g) and V_u (= 151.18 cm^3/mol) are the unit enthalpy and the unit volume of r-reg P3HT [46]. Importantly, the melting point depression is a function of three factors, ΔH_u, ϕ_1, and χ. In this work, we studied comparatively the effect of χ on T_m. As displayed in eq. 4, in front of χ, there is a negative sign, indicating that the smaller χ will results in a more depressed T_m. Here, if χ is small, it means that the intermolecular interactions [expressed by δ or (*cohesive energy density*)$^{1/2}$] in two different pure components, r-reg P3HT and PbI_2, are similar.

For example, as shown in Figure 10, in the case of the r-reg P3HT:PbI_2 system (DMSO), when χ(= 76.03 K/T) is relatively small, a more dramatic melting point depression is observed. However, in the case of the r-reg P3HT:PbI_2 system (DMF), the χ parameters are very close each other (665.38 K/T vs. 649.85 K/T) in the 1st and 18th steps, leading to a similar depression of melting points as proved in Fig. 10b. Note that, strictly speaking, the hydrophilic surface (step no. 18) in Fig. 10b exhibits a slightly smaller depression than the initial film (step no. 1). Hence, the aforementioned observation demonstrates that the Flory-Huggins theory with χ interaction parameter is useful for elucidating the interfacial interactions between two molecules or films (in this particular case, r-reg P3HT and PbI_2).

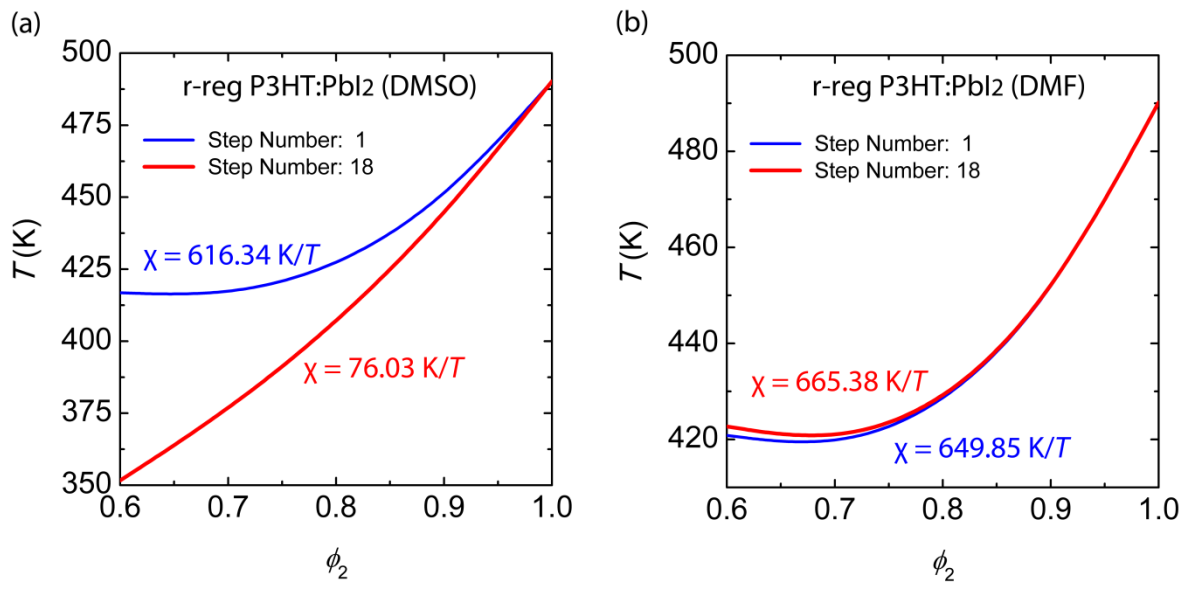

Figure 10.Melting point depression theory as a function of step number. (a) r-reg P3HT:PbI_2 system (when solvent is DMSO). (b) r-reg P3HT:PbI_2 system (when solvent is DMF).

4. CONCLUSION

Lead (II) iodide particles were synthesized via four different methods: hydrothermal, refluxing, solid-state reaction, and co-precipitation, showing unanimously the optical bandgap of 2.31 eV. When PbI_2 particles were characterized by XRD, they showed a hexagonal layered 2H structure, and the average crystallite size of 57±10 nm. Then PbI_2 films

were deposited on the top of mesoporous TiO_2 substrate using dipolar aprotic solvent, DMSO or DMF. The PbI_2 film (DSMO) showed a relatively homogeneous nanostructure, whereas the PbI_2 film (DMF) exhibited crack morphologies. Then the water contact angle was measured, leading to the solubility parameters, ca. 4.51-4.62 $(cal/cm^3)^{1/2}$. However, when the PbI_2 films were exposed to H_2O molecules in air, the solubility parameters were eventually changed into 7.28 $(cal/cm^3)^{1/2}$ for PbI_2(DMSO) and 12.98 $(cal/cm^3)^{1/2}$ for PbI_2(DMF), respectively. Finally, based on the theory of melting point depression combined with Flory-Huggins theory, we characterized the interfacial interactions between PbI_2 and r-reg P3HT. The PbI_2 film (DMSO) with χ= 76.03 K/*T*(e.g., χ= 0.26 at 298 K) showed dramatic melting point depression compared to the film (DMF) with χ= 665.38 K/*T* (e.g., χ= 2.23 at 298 K). These observations show that the Flory-Huggins theory with χ interaction parameter is still useful for understanding the interfacial interactions between a polymer (e.g., r-reg P3HT) and an inorganic film (e.g., PbI_2).Finally, we believe that our results offer a new insight for understanding solvent processing-structure-property relationship of PbI_2 thin-film, applicable to a sequential deposition method leading to high performance perovskite PVs.

Acknowledgment

N.A.is grateful to Jimma University, the Ministry of Education in Ethiopia, and Dean International Students Office at the Panjab University. G.V. acknowledges the financial assistance given by DST-UT(S&T&RE/RP/147/Sanc/09/2017/1123-1129), DST-PURSE, UGC-SAP, and TEQIP-III grants. We thank Dr. Timothy Kwa for contributing in the scientific discussion on the manuscript.

Conflict of Interest

The authors declare no competing financial interest.

References

[1] W. C.Fernelius, K. D. Detling,Preparation of crystals of sparingly soluble salts, J. Chem. Educ. 11 (1934) 176-178. https://doi.org/10.1021/ed011p176.

[2] H. Miyamae, Y. Numahata, M.Nagata,The crystal structure of lead(II) iodidie-dimethylsulphoxide(1/2) $PbI_2(dmso)_2$, Chem. Let. (1980) 663-664. https://doi.org/10.1246/cl.1980.663.

[3] H. L. Clever, The solubility of some sparingly soluble lead salts: An evaluation of the solubility in water and aqueous electrolyte solution, J. Phys. Chem. Ref. Data,9 (1980) 751-784.https://doi.org/10.1063/1.555628.

[4] C.W.J. Scaife, S.R.Cavoli, T.N. Blanton, M.D. Morse, B.R. Sever, W.S. Willis, S.L. Suib, Synthesis and characterization of lead(II) iodide grown in space, Chem. Mater. 2 (1990) 777-780.https://doi.org/10.1021/cm00012a034.

[5] A.F. da Silva, N. Veissid, C.Y. An, Optical determination of the direct bandgap energy of lead iodide crystals, Appl. Phys. Lett. 69 (1996) 1930-1932.https://doi.org/10.1063/1.117625.

[6] E. Lifshitz, M. Yassen, L. Bykov,I. Dag, R. Chaim, Photodecomposition and Regeneration of PbI_2 Nanometer-Sized Particles Embedded in Porous Silica Films, J. Phys. Chem. 99 (1995) 1245-1250. https://doi.org/10.1021/j100004a026.

[7] D. Ma, W. Zhang, R. Zhang, M. Zhang, G. Xi, Y. Qian, A facile hydrothermal synthesis route to single-crystalline lead iodide nanobelts and nanobelt bundles, J. Nanosci. Nanotechno. 5 (2005) 810-813. https://doi.org/10.1166/jnn.2005.142.

[8] X. Liu, S.T. Ha, Q. Zhang, M. de la Mata, C. Magen, J. Arbiol, T.C. Sum, Q.Xiong, Whispering Gallery Mode Lasing from Hexagonal Shaped Layered Lead Iodide Crystals, ACS Nano 9 (2015) 687-695. https://doi.org/10.1021/nn5061207.

[9] E. Klein, R. Lesyuk, C.Klinke, Insights into the formation mechanism of two-dimensional lead halide nanostructures, Nanoscale 10 (2018) 4442-4451.

https://doi.org/10.1039/C7NR09564C.

[10] C. Bacaksiz, H. Sahin,Single layer PbI_2: hydrogenation-driven reconstructions, RSC Adv. 6 (2016) 89708-89714. https://doi.org/10.1039/C6RA15020A.

[11] G. Popov, M.Mattinen, T.Hatanpää, M.Vehkamäki, M.Kemell, K.Mizohata, J. Räisänen, M.Ritala, M.Leskelä, Atomic Layer Deposition of PbI_2 Thin Films, Chem. Mater. 31 (2019) 1101-1109. https://doi.org/10.1021/acs.chemmater.8b04969.

[12] M.Schieberab, N.Zamoshchika, O.Khakhan, A.Zuck, Structural changes during vapor-phase deposition of polycrystalline-PbI_2 films, J. Cryst. Growth 310 (2008) 3168-3173. https://doi.org/10.1016/j.jcrysgro.2008.02.030.

[13] B. Pałosz, Reasons for Polytypism of Crystals of the Type MX_2. I. Polytypism and Structure Behaviour of Inorganic Crystals: General Problems, Phys. Status Solidi A77 (1983) 11-34. https://doi.org/10.1002/pssa.2210770102.

[14] P.A. Beckmann, A review of polytypism in lead iodide, Cryst. Res. Tech. 45 (2010) 455-460. https://doi.org/10.1002/crat.201000066.

[15] C.C. Coleman, H.Goldwhite, W. Tikkanen, A Review of Intercalation in Heavy Metal Iodides, Chem. Mater. 10 (1998) 2794-2800. https://doi.org/10.1021/cm980211r.

[16] I. Wharf, T. Gramstad, R. Makhija, M. Onyszchuk, Synthesis and vibrational spectra of some lead(II) halide adducts with O-, S-, and N-donor atom ligands, Can. J. Chem. 54 (1976) 3430-3438.https://doi.org/10.1139/v76-493.

[17]M. Shkir, S. AlFaify, Tailoring the structural, morphological, optical and dielectric properties of lead iodide through Nd^{3+} doping, Sci. Rep. 7 (2017) 16091. https://doi.org/10.1038/s41598-017-16086-x.

[18] S. Roth, W. R. Willig, Lead iodide nuclear particle detectors, Appl. Phys. Lett. 18 (1971) 328-330. https://doi.org/10.1063/1.1653682.

[19] W.R.Willig, Large bandgap mercury and lead compounds for nuclear particle detection,

Nucl.Instrum.Meth. 101 (1972) 23-24. https://doi.org/10.1016/0029-554X(72)90749-5.

[20] R.Minder, G.Ottaviani, C.Canali, Charge transport in layer semiconductors, J. Phys. Chem. Solids 37 (1976) 417-424. https://doi.org/10.1016/0022-3697(76)90023-8.

[21] J.Zhang, K.S.Shah, F.Olschner, J.C.Lund, L.P.Moy, K.Daley, L.Cirignano, M.R.Squillante, An improvement in growing large, oriented lead iodide single crystals for detector applications, Nucl. Instrum.Meth. A. 322 (1992) 499-503. https://doi.org/10.1016/0168-9002(92)91221-T.

[22] T.ESchlesinger, R.B. James, M. Schieber, J. Toney, J.M. van Scyoc, L. Salary, H. Hermon, J. Lund, A. Burger, K.-T. Chen, E. Cross, E. Soria, K. Shah, M. Squillante, H. Yoon, M. Goorsky, Characterization of lead iodide for nuclear spectrometers, Nucl. Instrum.Meth. A.380 (1996) 193-197. https://doi.org/10.1016/S0168-9002(96)00343-9.

[23] L.Fornaro, E.Saucedo, L.Mussio, L.Yerman, X.Ma, A.Burger, Lead iodide film deposition and characterization, Nucl. Instrum.Meth. A. 458 (2001) 406-412. https://doi.org/10.1016/S0168-9002(00)00933-5.

[24] G. Zhu, M.Hojamberdiev, P. Liu, J. Peng, J. Zhou, X.Bian, X. Huang, The effects of synthesis parameters on the formation of PbI_2 particles under DTAB-assisted hydrothermal process, Mater. Chem. Phys. 131 (2011) 64-67. https://doi.org/10.1016/j.matchemphys.2011.07.010.

[25] J.Tonn, M.Matuchova, A.N.Danilewsky, A.Cröll, Removal of oxidic impurities for the growth of high purity lead iodide single crystals, J. Cryst. Growth 416 (2015) 82-89. https://doi.org/10.1016/j.jcrysgro.2015.01.024.

[26] S.-Y. Kim, H. J. Jo, S.-J.Sung, D.-H. Kim, Perspective: Understanding of ripening growth model for minimum residual PbI_2 and its limitation in the planar perovskite solar cells, APL Mater. 4 (2016) 100901.https://doi.org/10.1063/1.4963841.

[27] M. Shkir, I.S.Yahia, V. Ganesh, Y. Bitla, I.M. Ashraf, A. Kaushik, S. AlFaify, A facile

synthesis of Au-nanoparticles decorated PbI_2 single crystalline nanosheets for optoelectronic device applications, Sci. Rep. 8 (2018) 13806. https://doi.org/10.1038/s41598-018-32038-5.

[28] A. Kojima, K. Teshima, Y. Shirai, T. Miyasaka, Organometal Halide Perovskites as Visible-Light Sensitizers for Photovoltaic Cells, J. Am. Chem. Soc. 131 (2009), 6050-6051. https://doi.org/10.1021/ja809598r.

[29] N. Ahn, D.-Y.Son, I.-H.Jang, S. M. Kang, M. Choi, N.-G. Park, Highly Reproducible Perovskite Solar Cells with Average Efficiency of 18.3% and Best Efficiency of 19.7% Fabricated via Lewis Base Adduct of Lead(II) Iodide, J. Am. Chem. Soc. 137 (2015) 8696-8699. https://doi.org/10.1021/jacs.5b04930.

[30] J. S. Manser, M. I. Saidaminov, J.A. Christians, O.M. Bakr, P.V. Kamat, Making and Breaking of Lead Halide Perovskites, Acc. Chem. Res. 49 (2016) 330-338. https://doi.org/10.1021/acs.accounts.5b00455.

[31] M. M. Lee, J. Teuscher, T. Miyasaka, T. N. Murakami, H. J. Snaith, Efficient Hybrid Solar Cells Based on Meso-Superstructured Organometal Halide Perovskites, Science, 338 (2012), 643-647. https://doi.org/10.1126/science.1228604.

[32] J. Burschka, N. Pellet, S.-J. Moon, R. Humphry-Baker, P. Gao, M. K. Nazeeruddin, M. Grätzel, Sequential deposition as a route to high-performance perovskite-sensitized solar cells,Nature499 (2013) 316–319.https://doi.org/10.1038/nature12340.

[33] F. Sahli, J. Werner, B. A. Kamino, M. Bräuninger, R. Monnard, B. Paviet-Salomon, L. Barraud, L. Ding, J. J. D. Leon, D. Sacchetto, G. Cattaneo, M. Despeisse, M. Boccard, S. Nicolay, Q. Jeangros, B. Niesen, C. Ballif, Fully textured monolithic perovskite/silicon tandem solar cells with 25.2% power conversion efficiency, Nat. Mater. 17 (2018) 820-826. https://doi.org/10.1038/s41563-018-0115-4.

[34]P. J. Flory, Principles of Polymer Chemistry; Cornell University Press, Ithaca,NY, 1953.

[35]K. Kaviyarasu, D. Sajan, M.S. Selvakumar, S.A. Thomas, D.P. Anand, A facile

hydrothermal route to synthesize novel PbI_2nanorods, J. Phys. Chem. Solids 73 (2012) 1396-1400. https://doi.org/10.1016/j.jpcs.2012.06.005.

[36]T.D.Malevu, R.O.Ocaya, K.G.Tshabalala, Phase transformations of high-purity PbI_2 nanoparticles synthesized from lead-acid accumulator anodes, Physica B 496 (2016) 69-73. https://doi.org/10.1016/j.physb.2016.05.027.

[37]R.J.M.Konings, E.H.P.Cordfunke, R.R.van der Laan, Enthalpy increment measurements of PbI_2: evidence for a reversible polytypic transition, J. Alloys Compd.230 (1995) 85-88. https://doi.org/10.1016/0925-8388(95)01898-0.

[38]B.D. Cullity, S.R. Stock, Elements of X-Ray Diffraction, Prentice Hall,Upper Saddle River,NJ, 2001.

[39] M.V. Artemyev, G.P. Yablonski, Y.P. Rakovich, Luminescence Spectra of Quantum-Sized CdS and PbI_2 Particles in Static Electric Field, 87 (1995) 523-527. https://doi.org/10.12693/APhysPolA.87.523.

[40]M. Belmares, M. Blanco, W.A. Goddard III, R.B. Ross, G. Caldwell, S.□H. Chou, J. Pham, P.M. Olofson, C. Thomas, Hildebrand and Hansen solubility parameters from Molecular Dynamics with applications to electronic nose polymer sensors, J. Comput. Chem. 25 (2004) 1814-1826. https://doi.org/10.1002/jcc.20098.

[41]R.C. Weast, CRC Handbook of Chemistry and Physics, 77 ed., CRC Press, Boca Raton, FL, 1996.

[42] P. Patnaik, Handbook of Inorganic Chemicals, McGraw-Hill, Burlington, NJ,2003.

[43]D. Li, A.W. Neumann, A Reformulation of the Equation of State for Interfacial Tensions, J. Colloid Interface Sci. 137 (1990) 304-307. https://doi.org/10.1016/0021-9797(90)90067-X.

[44] D. Li, A.W. Neumann, Contact Angles on Hydrophobic Solid Surfaces and Their Interpretation. J. Colloid. Interface Sci. 148 (1992) 190-200.https://doi.org/10.1016/0021-9797(92)90127-8.

[45] S. Nilsson, A. Bernasik, A. Budkowski, E. Moons, Morphology and Phase Separation of Spin-Coated Films of Polyfluorene/PCBM Blends, Macromolecules 40 (2007) 8291-8301.https://doi.org/10.1021/ma070712a.

[46]J.Y. Kim, Order-Disorder Phase Equilibria of Regioregular Poly(3-hexylthiophene-2,5,diyl) Solution,Macromolecules 51 (2018) 9026–9034. https://doi.org/10.1021/acs.macromol.8b01498.

[47] J.Y. Kim, Phase Diagrams of Binary Low Bandgap Conjugated Polymer Solutions and Blends, Macromolecules 52 (2019) 4317-4328. https://doi.org/10.1021/acs.macromol.9b00477.

[48] P.C.Hiemenz, T.P. Lodge, Polymer Chemistry, second ed., CRC Press Taylor & Francis Group, Boca Raton, FL, 2007.

Graphical Abstract

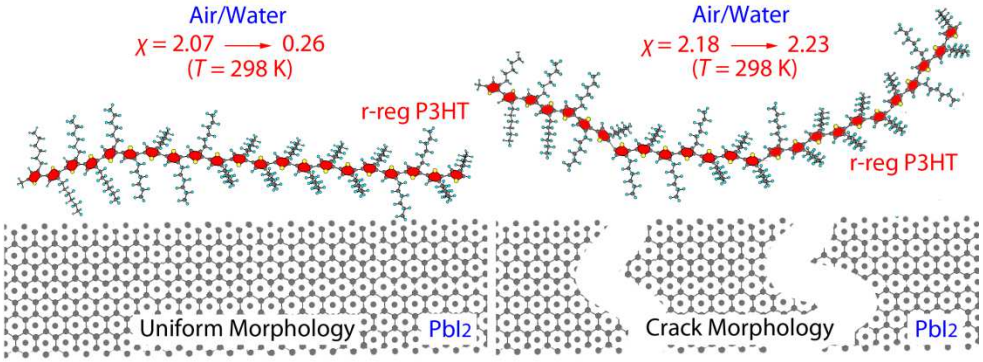

Highlights

- PbI_2 particles were successfully synthesized through versatile synthesis methods (hydrothermal, refluxing, solid-state reaction, and co-precipitation), exhibiting hexagonal layered 2H structure with particle size 57±10 nm and the optical bandgap of 2.31 eV.
- The surface properties (morphology, surface tension, solubility parameter) of nanostructural PbI_2 films deposited on the top of mesoporous TiO_2 are dependent on the processing solvents (DMSO and DMF).
- The interfacial interactions between PbI_2 and r-reg P3HT were characterized successfully based on the theory of melting point dispersion combined with Flory-Huggins theory.
- The PbI_2 film (DMSO) with χ= 76.03 K/T(e.g., χ= 0.26 at 298 K) showed dramatic melting point depression compared to the film (DMF) with χ= 665.38 K/T (e.g., χ= 2.23 at 298 K).
- The Flory-Huggins theory with χ interaction parameter is still useful for understanding the interfacial interactions between a polymer (e.g., r-reg P3HT) and an inorganic film (e.g., PbI_2).

Author declaration

[Instructions: Please check all applicable boxes and provide additional information as requested.]

1. Conflict of Interest

Potential conflict of interest exists:

We wish to draw the attention of the Editor to the following facts, which may be considered as potential conflicts of interest, and to significant financial contributions to this work:

The nature of potential conflict of interest is described below:

☐No conflict of interest exists.

We wish to confirm that there are no known conflicts of interest associated with this publication and there has been no significant financial support for this work that could have influenced its outcome.

2. Funding

☐Funding was received for this work.

All of the sources of funding for the work described in this publication are acknowledged below:

[List funding sources and their role in study design, data analysis, and result interpretation]

Ethiopian Ministry of Education

TEQIP-III, UGC SAP, DST PURSE and DST UT Chandigarh grants were used.

3. Intellectual Property

☐We confirm that we have given due consideration to the protection of intellectual property associated with this work and that there are no impediments to publication, including the timing of publication, with respect to intellectual property. In so doing we confirm that we have followed the regulations of our institutions concerning intellectual property.

4. Research Ethics

☐We further confirm that any aspect of the work covered in this manuscript that has involved human patients has been conducted with the ethical approval of all relevant bodies and that such approvals are acknowledged within the manuscript.

☐IRB approval was obtained (required for studies and series of 3 or more cases)

☐Written consent to publish potentially identifying information, such as details or the case and photographs, was obtained from the patient(s) or their legal guardian(s).

5. Authorship

The International Committee of Medical Journal Editors (ICMJE) recommends that authorship be based on the following four criteria:

1. Substantial contributions to the conception or design of the work; or the acquisition, analysis, or interpretation of data for the work; AND
2. Drafting the work or revising it critically for important intellectual content; AND
3. Final approval of the version to be published; AND
4. Agreement to be accountable for all aspects of the work in ensuring that questions related to the accuracy or integrity of any part of the work are appropriately investigated and resolved.

All those designated as authors should meet all four criteria for authorship, and all who meet the four criteria should be identified as authors. For more information on authorship, please see http://www.icmje.org/recommendations/browse/roles-and-responsibilities/defining-the-role-of-authors-and-contributors.html#two.

We believe these individuals should be listed as authors because:

Ahmed, Nasir Awol; Geffe, Chernet Amente; Verma, Gaurav; Kim, Jung Yong

☐We confirm that the manuscript has been read and approved by all named authors.

☐We confirm that the order of authors listed in the manuscript has been approved by all named authors.

6. Contact with the Editorial Office

The Corresponding Author declared on the title page of the manuscriptis:

Gaurav Verma

☐This author submitted this manuscript using his/her account in EVISE.

☐We understand that this Corresponding Author is the sole contact for the Editorial process (including EVISE and direct communications with the office). He/she is responsible for communicating with the other authors about progress, submissions of revisions and final approval of proofs.

☐We confirm that the email address shown below is accessible by the Corresponding Author, is the address to which Corresponding Author's EVISE account is linked, and has been configured to accept email from the editorial office of American Journal of Ophthalmology Case Reports:

gauravvermas@gmail.com; gauravverma@pu.ac.in

☐We understand that this author is the sole contact for the Editorial process (including EVISE and direct communications with the office). He is responsible for communicating with the other authors, including the Corresponding Author, about progress, submissions of revisions and final approval of proofs.

We the undersigned agree with all of the above.

Author's name (Fist, Last)	Signature	Date
1. Gaurav, Verma		28 Jan 2020
2. Jung Yong, Kim_____		28 Jan 2020
3. Nasir Awol , Ahmed		28 Jan 2020
4. Chernet Amente, Geffe		28 Jan 2020